Mesoscopic real space structures in spin-glass aging: the Edwards-Anderson model.

Paolo Sibani[1] and Stefan Boettcher[2]

[1]*FKF, University of Southern Denmark, Campusvej 55, DK5230, Odense M, Denmark*
[2]*Department of Physics, Emory University, Atlanta, GA 30322, USA.*

Isothermal simulational data for the 3D Edwards-Anderson spin glass are collected at several temperatures below T_c and, in analogy with a recent model of dense colloidal suspensions, interpreted in terms of clusters of contiguous spins overturned by quakes, non-equilibrium events linked to record sized energy fluctuations. We show numerically that, to a good approximation, these quakes are statistically independent and constitute a Poisson process whose average grows logarithmically in time. The overturned clusters are local projections on one of the two ground states of the model, and grow likewise logarithmically in time. Data collected at different temperatures T can be collapsed by scaling them with $T^{-1.75}$, a hitherto unnoticed feature of the E-A model, which we relate on the one hand to the geometry of configuration space and on the other to experimental memory and rejuvenation effects. The rate at which a cluster flips is shown to decrease exponentially with the size of the cluster, as recently assumed in a coarse grained model of dense colloidal dynamics. The evolving structure of clusters in real space is finally ssociated to the decay of the thermo-remanent magnetization. Our analysis provides an unconventional coarse-grained description of spin glass aging as statistically subordinated to a Poisson quaking process and highlights record dynamics as a viable common theoretical framework for aging in different systems.

I. INTRODUCTION

Intensely investigated in the last few decades, the multi-scale dynamical process called *aging* is widely observed in glassy systems subject to a change of an external parameter, e.g. a thermal quench. While spin-glasses [1–4], colloidal suspensions [5], vortices in superconductors [6], magnetic nanoparticles in a ferrofluid [7] and ecosystems [8, 9] may have little in common in terms of microscopic variables and interactions, strong similarities emerge in their aging phenomenology. For example, one point averages feature a logarithmic time dependence [10] which entails an asymptotically vanishing rate of change of the corresponding observables and clarifies why aging systems deceptively appear in equilibrium for observation times shorter than their age. Secondly, two-time averages such as correlation and response functions often possess an approximate dependence on the single scaling variable t/t_w [11]. Interestingly, this property is shared by the probability that a species is extant at times t_w and $t > t_w$ in a model of biological evolution [9].

Thermal relaxation models associate the multi-scaled nature of aging processes to a hierarchy of metastable components of configuration space [12–14], often described as nested 'valleys' of an energy landscape. Local thermal equilibration is described in terms of time dependent valley occupation probabilities [15], which are controlled by transition rates over the available 'passes'. When applied to a hierarchical structure, such description gradually coarsens over time as valleys of increasing size reach equilibrium. That barrier crossings are connected to record values in time series of sampled energies [20, 21] is a central point in record dynamics (RD), a coarse-grained description of aging which uses the statistics of non-equilibrium events called *quakes* to describe

aging in different settings [16–19].

In connection with spin-glasses, RD has predictions describing Thermo-Remanent Magnetization (TRM) data [17] and explaining their observed *sub-aging* behavior [11], i.e. their deviation from t/t_w scaling. In this work we explicitly check its basic assumptions and use it to provide a different perspective on an iconic model of glassy behavior, the Edwards-Anderson (EA) spin-glass [22].

Usually more reliant on system specific details than their more abstract configuration space counterparts, real-space models often build on the properties of domains whose time dependent linear size $l(T, t)$ characterizes the aging process, see e.g. [7, 23]. Independent of the mechanism assumed for domain growth, degrees of freedom belonging to the same domain are assumed to fluctuate around their thermal equilibrium state, while those located in different domains have, for a fixed time scale, frozen relative orientations. The functional form of $l(T, t)$ can be extracted from simulational data using a four-point equilibrium correlation function [23].

Specifically in the spin glass droplet model [1], domains are defined in terms of projections onto the two available ground states. Since the time growth of $l(T, t)$ minimizes the free energy by decreasing the domain wall length, the droplet model views domain growth in a spin glass as homologous to the scale-free coarsening process of a ferromagnet at its critical temperature.

Note however that, while the interior of a ferromagnetic domain only harbors local excitations of the ground state, analyses of small short-ranged spin glass systems [24] indicate that each domain accommodates a multitude of metastable configurations. The same conclusion can be reached from a more recent enumeration of all the metastable configurations of E-A models of differ-

ent linear sizes [25]. It thus seems questionable that domain walls provide the main contribution to free energy barriers in a spin glass. Finally, the droplet model leaves no room for the temporally intermittent and spatially heterogeneous events now recognized as key features of glassy dynamics [26].

From data analyses, real space length scales in aging systems are linked to the equilibrium correlation length of their metastable states, and recent numerical [27, 28] and experimental [30, 31] efforts utilize correlation and response functions to describe the growth of correlated domains. Inspired by a recent model of colloidal aging [32, 33], we use a different approach to identify growing real space structures in the E-A spin glass and argue that these are the coarsening variables controlling aging by linking them to TRM data.

In models of dense colloids [32, 33] clusters of contiguous particles, which gradually grow by accretion and suddenly collapse through quakes, fullfill this dynamical role, while the microscopic particle motion is only described statistically through a size dependent cluster collapse rate. The crucial assumption that this rate decreases exponentially with cluster size, corresponding to the likelihood of a spontaneous fluctuation of that size, reproduces the available numerical and experimental evidence on dense hard sphere colloids. As well, pertinent RD predictions, including a logarithmic time growth of the average cluster size, are obtained. A recent re-analysis [34] of experimental evidence shows that the quaking rate in dense colloidal suspensions decreases as $1/t$, which is the basic claim from which RD predictions flow. The experimental evidence was confirmed with molecular dynamics simulations of such a colloid [35].

To buttress our hypothesis, we analyze, as anticipated, the dynamics of the E-A spin-glass [22], a model with quenched randomness microscopically very different from a dense colloid. Its very well studied behavior is usually associated with two competing theoretical approaches [1, 36, 37] which, in spite of their differences, share conceptual roots in the equilibrium statistical mechanics of critical phenomena. A unified description of aging phenomenology requires, we believe, a much stronger focus on the statistics of the rare nonequilibrium events that drive the dynamics in the full range of parameters, e.g. temperature or density, where aging is observed.

Our simulations show: *i)* That the energy changes associated to quakes stand out from the overwhelming majority of energy fluctuations. *ii)* That quakes are statistically uncorrelated and occur at a rate which is constant in *logarithmic time*, as predicted by RD. *iii)* That suitably defined clusters grow on average in proportion to $\ln t$. The last result concurs with the behavior observed in [32, 33] for a model of colloids. Provided that the cluster size distribution is sufficiently peaked around its mean, it also supports the latter model hypothesis that

clusters are overturned at a rate exponentially decreasing with their size. Last but not least, our analysis provides an approximate description of spin glass dynamics in terms of flipping clusters which is more complete than previously available and covers the TRM decay behavior.

The rest of the paper is organized as follows: In Section II the E-A model definition is stated for the reader's convenience. In Section III we summarize the theoretical concepts used in our data analysis. Our numerical results are presented in Section IV and a real space coarse grained description of the E-A spin glass dynamics is given in Section V. Finally, Section VI highlights similarities between our observed T scaling of energy fluctuations and experimental memory and rejuvenation properties of spin glasses. Section VII provides a summary and draws conclusions.

II. MODEL

We consider an Ising E-A spin glass [22] placed on a cubic grid with linear size $L = 20$ and periodic boundary conditions. Each of the 2^N configurations is specified by the value of $N = L^3$ dichotomic spins, and has, in zero magnetic field, an energy given by

$$H(\sigma_1, \sigma_2, \ldots \sigma_N) = \frac{1}{2} \sum_{i=1}^{N} \sum_{j \in \mathcal{N}(i)} J_{ij} \sigma_i \sigma_j, \qquad (1)$$

where $\sigma_i = \pm 1$ and where $\mathcal{N}(i)$ denotes the six nearest neighbors of spin i. For $j < i$, the J_{ij}s are drawn independently from a Gaussian distribution with zero average and unit variance. Finally, $J_{ij} = J_{ji}$ and $J_{ii} = 0$. All parameters are treated as dimensionless. This model has a phase transition from a paramagnetic to a spin-glass phase at critical temperature which in Ref. [38] is estimated to be $T_c = 0.9508$. The same reference reviews the different T_c estimates found in the literature.

III. METHOD OF ANALYSIS

Starting from a configuration previously equilibrated at temperature $T_0 = 1.25$, the system is instantaneously quenched at time $t = 0$ down to $T < 1$. The ensuing aging process is then followed for five decades in time. For aging temperature $T = .3, .4, .5, .6, .7, .75$ and $.8$, 512 independent simulations are carried out and special events, the quakes, are extracted from the trajectories thus obtained. After defining a detection criterion (see below), we check that quake events are uncorrelated and Poisson distributed with an average proportional to $\ln t$. We then identify clusters of spins that move in unison during the quakes, and from those construct the average cluster size, $S_{\mathrm{Cl}}(t)$, as a function of time.

The Waiting Time Method [39] (WTM), a kinetic MC algorithm which performs single spin flips with no rejections, is used in all simulations. Similarly to the more widely used Metropolis algorithm and its more recent variants, e.g. parallel tempering [40], the WTM fulfils the detailed balance condition, and is by design guaranteed to eventually sample the equilibrium distribution of the problem at hand. Its performance in exploring the EA energy landscape at low T was compared in Ref. [21] to that of Extremal Optimization [41]. These two very different methods extracted the same geometrical features from the landscape, e.g. that a record high energy barrier must be scaled in order to find a lower value of the lowest energy seen 'so far', or 'best so far energy' E_{bsf} to which we shall return. Being calculated along the trajectories as differences between the energy of the current state and the E_{bsf}, the above barriers differ conceptually from the overlap barriers investigated in Refs. [42], which describe displacement fluctuations in thermal equilibrium.

In a jammed system as an aging spin-glass, Metropolis executes a large number of unsuccessful trials (and the acceptance rate drastically declines), which the WTM avoids by rank-ordering the execution time of all possible moves and then executing the one with the lowest execution time. Specifically, flipping spin i at energy cost δ_i is associated to a waiting time w_i and the intrinsic time variable t (flipping time) of the WTM is a real positive number which sums up, at any point of the simulation, the times spent 'waiting' for all previous flips. Each waiting time is drawn from an exponential distribution with average

$$\langle w_i \rangle = \exp(\frac{\delta_i}{2T}). \qquad (2)$$

Hence, as long as its local environment remains unchanged, the thermal flips of each spin are a memoryless Poisson process with the above average. This seems a physically appealing description of systems with many coupled degrees of freedom and implies that, when a spin is reversed, only the waiting and flipping times of that spin and its neighbors need to be recalculated, while all others can stay put.

Both the WTM and the Metropolis algorithm lack a physical time scale, and their ability to empirically describe aging processes depends on the temporal scale invariance of such processes, combined with the fact that both methods seek the pseudo-equilibrium states in which aging system dwell most of the time. Once the Metropolis algorithm has had a chance to query every spin, it flips a set of spins similar to that flipped by the WTM. For times of the order of a MC sweep or larger, the two methods are equivalent and our t corresponds to the number of MC sweeps [39].

The sequence of flips is however clearly different, since Metropolis chooses the 'next' flip candidate at random, while each choice of the WTM can be influenced by the last flip: Equation (2) implies that any negative 'barrier' δ_i which arise after a move creates a locally unstable situation where the involved spins quickly flip. This process can iteratively generate a series of negative δ_i values in a local neighborhood, triggering event cascades whose short duration allows one to time-stamp quakes with high resolution. The latter feature is important when assessing the temporal statistics of the quakes. Besides being computationally inefficient at low T, a Metropolis algorithm would express 'times' as integer number of sweeps, which is at variance with time being a real variable in a Poisson process. In contrast, WTM readily resolves sub-sweep timescales.

For short time intervals and at low temperatures, the WTM dwells in real space neighborhoods of local energy minima, and the sampled energy changes feature a previously unnoticed temperature scaling which is found in most of our figures and explained in Section IV C in terms of the distribution of single flip energy changes available near local energy minima.

Clusters and domains

A local energy minimum configuration consists of disjoint groups of contiguous spins, our clusters, whose orientation is either the same or the opposite as one of the two ground states, if one neglects, as we presently do, the spins on the cluster boundaries. Since each cluster may contain sub-clusters of opposite orientation, a partially nested structure is generated, reflecting the degree of hierarchical organization of the system's configuration space [14, 24]. The situation is illustrated in Fig. 1, using two dimensions for graphical convenience. Excess energy relative to the ground state stems from cluster interfaces and can be reduced in a thermally activated process overturning gradually larger clusters. The free energy cost of such reversals is mainly associated with barriers in the bulk of each cluster, as we will explain below. In contrast, the cost of overturning a ferromagnetic domain is mainly associated with the domain's interface.

Quickly reversible single spin flips similar to 'in cage rattlings' in a colloid are excluded from cluster configurations. Their long term effects are subsumed into the statistics of the quakes which provide the elementary moves, i.e. cluster flips, of the coarse-grained dynamics we are about to describe. Since spins move together in a quake, the final configurations of two successive quakes are compared, all spins which changed orientation are identified and grouped into clusters of spatially contiguous elements. Finally, clusters with less than 5 spins are discarded to minimize the risk of erroneously counting reversible moves as part of a quake.
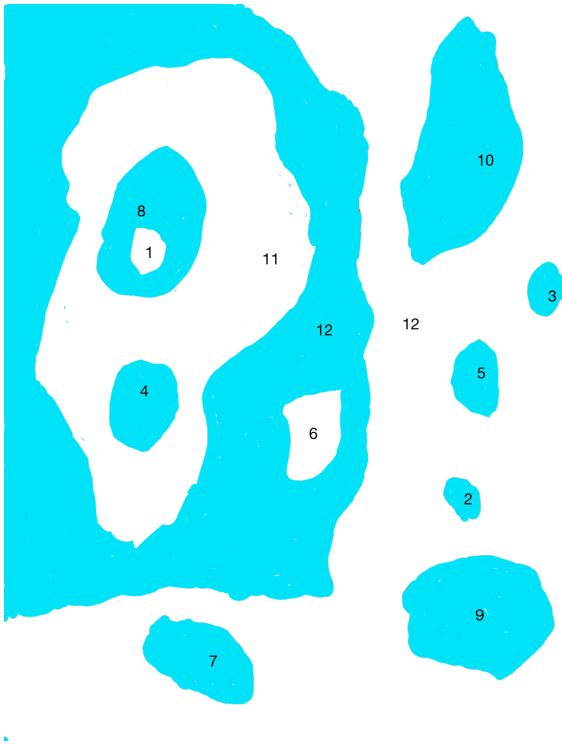
Figure 1. Depiction of the domain hierarchy in a hyperplane of a 3d-Edwards-Anderson spin glass during the aging process. Each numbered area represents spin clusters with the same configuration as one of the two ground states of the E-A spin glass. With the exception of area 12, which has two colors, each cluster is surrounded by a region of the opposite color and takes up this color when overturned by a quake. In this picture, randomly fluctuating, isolated spins have been suppressed. A quake event amounts to filling in one of the inner-most domains through flipping all its spins, thereby coarsening the otherwise self-similar spatial hierarchy of domains-within-domains.

Quake detection protocol

Observation of non-equilibrium phenomena is fundamentally tied to choosing the correct time and length scales. This applies certainly to the aging process. On very large scales macroscopic variables seem to change in a smooth and gradual manner. On intermediate scales aging systems appear in a state of quasi-equilibrium punctuated by increasingly rare, intermittent quakes that significantly (i.e., irreversibly) relax the system and lead to overall structural changes. The importance of these events for the progression of the aging process was highlighted in [43] using a system-wide approach. However, since quakes unfold almost instantaneously on an intermediate time-scale, a more detailed investigation is needed to explore the *spatial* dynamic that facilitates the quake. In the following we outline a protocol to zoom in more closely into a narrower time-window, as illustrated in Fig. 3, where the quake's footprint is measured from the difference between the configuration it generates and that it inherits previous quake, see Fig. (1). This contrasts with equivalent aging experiments on structural glasses such as colloids, where spatial traces of quakes are faint.

Our method of data analysis identifies quakes on the fly from an evolving trajectory and treats them, approximately, as instantaneous events. The identification process involves a number of computational choices, which are all based on the following assumptions: Using $\ln(t)$ rather than t as independent variable transforms the quakes into a memoryless Poisson process. Accordingly, successive quakes are statistically independent, and if t_k is the time of occurrence of the kth quake, the 'logarithmic waiting times' $\Delta\ln_k = \ln(t_k) - \ln(t_{k-1}) = \ln(t_k/t_{k-1})$ are independent stochastic variables with the same exponential distribution. Correspondingly, the logarithmic rate of quakes is constant.

In Ref. [43, 44] energy differences were sampled over time intervals of duration δt, chosen much smaller than the system age but larger than the decay time of the energy autocorrelation function. On this intermediate time-scale, intermittent events were distinguished from equilibrium fluctuations based on their correspondence to rare, negative and numerically large energy changes without resolving the quake event itself. In our case, we provide precise values for the onset times of quakes by explicitly connecting them to the extremal value of the 'energy barrier' function discussed in Refs. [20, 21]. For that purpose, energy changes in close proximity of local energy minima are monitored by choosing δt now much *shorter* than the energy autocorrelation decay time, such that neither equilibrium fluctuations nor quakes can unfold within a single δt. Energy changes measured within such a short δt without reference to barrier-height feature a perfect normal distribution over many orders of magnitude, see Fig. (4). That the width of this distribution scales anomalously with with temperature confirms that the energy changes sampled are not equilibrium fluctuations.

In contrast, to capture an actual quake, we have to use a specific trigger, described in Figs. 2 and 3. Following Refs. [20, 21], we consider the barrier function $b(t) = E(t) - E_{\text{bsf}}(t)$, where $E_{\text{bsf}}(t) = \min_t[E(t)]$ is the lowest energy ever seen up to time t. According to Ref. [20], the entry and exit times of a trajectory in and out of a valley in the energy landscape can be evinced from the sequence of configurations where $b(t)$ and $E_{\text{bsf}}(t)$ reach their maxima and minima, respectively. As the description in Fig. 2 demonstrates, the most recent barrier record B_i only becomes recognized as such when the next minimum is reached and, correspondingly, the latest E_i is certified as such only after $b(t)$ achieves a new record. Thus, this classification scheme requires a-priori knowledge of the entire time series of energy values, which we want to avoid. Furthermore, we do not
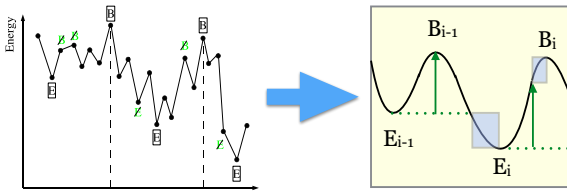
Figure 2. The instantaneous energy $E(t)$ of the system fluctuates widely while decaying slowly overall (left panel). The lowest energy $E_{\mathrm{bsf}}(t) = \min_t[E(t)]$, and the highest barrier $\max_t[E(t) - E_{\mathrm{bsf}}(t)]$ ever seen up to time t are marked by E and B, respectively. In Refs. [20, 21], intermediate records were stricken (crossed-out green letters) and the last B-record before the next E, or the last E-record before the next B were kept to coarse-grain the states visited into "valleys" entered and exited at barrier-crossings B_{i-1} and B_i and to demarcate the catchment basin of the local minimum at E_i, as shown in the right panel. Here, we focus on the record-producing parts of the trajectory enclosed in the shaded boxes. In the lower box $E(t)$ begins to undercut the previous minimum, E_{i-1}, until E_i is reached and in the upper box it exceeds the previous barrier record (up-arrow) until B_i is reached.
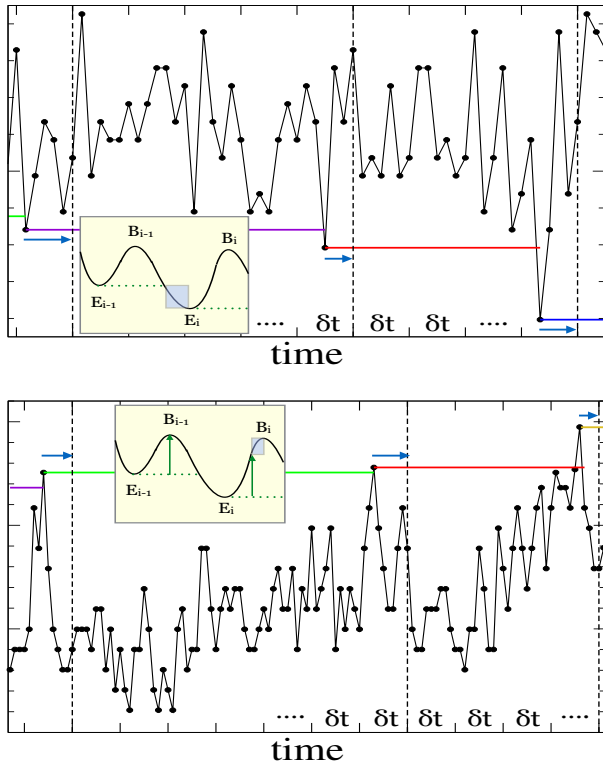

Figure 3. On-the-fly detection of quakes while reaching new energy minima E_i (top panel) or barrier records B_i (bottom panel). Within the respective ranges (shaded boxes in insets), a progression of new records, either of $E_{\mathrm{bsf}}(t)$ (top) or of $b(t)$ (bottom), is reached through quakes. In top (bottom) panel, once the energy signal reaches below (above) the previous record, a quake event commences, marked by a colored horizontal line. To capture the footprint of such a quake, we record the spin configuration at the end of those time-intervals δt that contain a record (vertical dashed lines). The spin orientation changes between consecutive quakes provide the spatial extent of the intervening quake. The sub-interval duration δt used in the simulation is $\delta t = 0.999$.

only focus on exit and entry points of valleys in configuration space, but wish to identify the spatially localized non-equilibrium events which provide the path approaching E_i and B_i, respectively marked by a shaded box in the insets of Fig. 2. Approaching E_i, $E(t)$ achieves a sequence of new $E_{\mathrm{bsf}}(t)$ after the latest record barrier crossing. In turn, the function $b(t)$ reaches new records after the latest minimum $E_{\mathrm{bsf}}(t)$ become fixed and B_i is approached. Typical sequences of $E(t)$ within those regimes are depicted in the main panels of Fig. 3. For either regime, we stipulate that, if $E_{\mathrm{bsf}}(t)$ or $b(t)$ achieve a new record value at $t = t_r$, a quake is unfolding. As soon as t then reaches the upper boundary of the sub-interval containing t_r, i.e., $t \leq t_r < t + \delta t$, that quake is deemed to have ended and the system's configuration is saved. We then repeat this procedure for the next record, until E_i or B_i, respectively, is reached and continue the process in valley $i + 1$ at later times. From the energy differences $\delta E_q(i)$, $i = 1, 2 \ldots N$ between the current and the previously saved configurations one easily finds the total energy change connected to the quake and the positions of the participating spins. The statistical error in the procedure comes from unrelated spins which flip and participating spins which flip twice.

The above detection scheme allows a precise assessment of quake times, and does not use threshold values to discriminate quakes from quasi-equilibrium thermal fluctuations. The arbitrary subdivision of the observation interval into sub-intervals of length δt determines when a quake ends, but has only a minor effect on the measured values of inter-quakes times, which are typically much longer than δt. Finally, reaching the different energy records which define our quake detection technique also requires tortuous paths, which are tantamount to entropic barriers. These are not shown in Figs. 2-3, but are important for the dynamics, as argued in Section IV C.

To conclude, the WTM is ideally suited for our measurements. It produces equivalent physical results to random sequential MC, yet, WTM focuses more efficiently on the few active spins that drive the dynamics. By ranking degrees of freedom by their time for change, it targets on exactly those spins connected within a quake and is able to time-stamp quakes with high accuracy.

IV. NUMERICAL RESULTS

After the initial quench $T = 1.25 \rightarrow T < 1$, the system is aged up to time $t_{\mathrm{w}} = 100$ without taking any data. Data are taken in the interval $[t_{\mathrm{w}}, 10^5]$ which is subdivided into 10^5 subintervals of duration $\delta t = 0.999$. This duration is an upper bound for the temporal resolution of quake times, as explained in the 'Quake detection protocol' section above. As mentioned, 512 independent simulations are carried out for statistical reasons, all starting from the same equilibrium configuration.

The first two subsections below detail different types of simulational results, and the last subsection rationalizes the T scaling form used to collapse all our data. All quantities specified below are dimensionless.

Mathematical symbols used	
T, t	Temperature and time
δt	Short time interval
Δ	Energy change over δt
Δ_q	Quake induced energy change
$\Delta \ln$	Logarithmic waiting time
r_q	Logarithmic quaking rate
$R_q(t)$	Quaking rate $= r_q/t$
r_{cl}	Logarithmic rate of cluster growth
$n_q(t)$	Number of quakes up to time t
$\mathbf{F}_A(x)$	PDF of stochastic variable A

A. Energy fluctuations PDFs

Energy fluctuations sampled during isothermal aging at constant temperature T have PDFs which change widely with T. As one would expect, the fluctuations are smaller the lower the temperature. Interestingly, their scaling is not linear in T, as would be the case when dealing with equilibrium energy fluctuations, but involves instead the power law T^α, where $\alpha = 1.75$. Let $T^{-\alpha}\Delta$ denote the scaled energy changes (per spin) sampled at temperature T over an interval of a very short duration $\delta t = 0.999$. The length of this interval, which is much shorter than those considered in [43] and far too short to straddle equilibrium like energy fluctuations, provides an upper bound for the duration of 'instantaneous' quakes.

The seven estimated PDFs of $T^{-\alpha}\Delta$, sampled at seven different aging temperatures $T = .3, .4, \ldots .7, .75$ and $.8$, are plotted in Fig. 4 using a light color (yellow) and using, in order of increasing T, squares, circles, diamonds, hexagrams, pentagrams, and down- and up-pointing triangles as symbols. The dotted line is a fit of all these scaled PDFs to a Gaussian of zero average. We note that the data collapse is excellent and that the standard deviation of the Gaussian $\sigma_G \approx 6.2 \ 10^{-3}$ is much smaller than unity, the statistical spread of the coupling constants J_{ij}. This confirms that the sampled energy changes are strongly constrained, as expected.

Quake induced energy changes Δ_q occur over the time intervals of varying length which stretch from one quake to the next. Positive and negative values of Δ_q are associated with the system's energy increasing or decreasing beyond its previous maximum or minimum, respectively. The average effect of a quake is however an energy loss.

The empirical PDFs of $T^{-\alpha}\Delta_q$ are shown using the same symbols as for the Gaussian changes, but a darker color (red). For negative values of the abscissa these
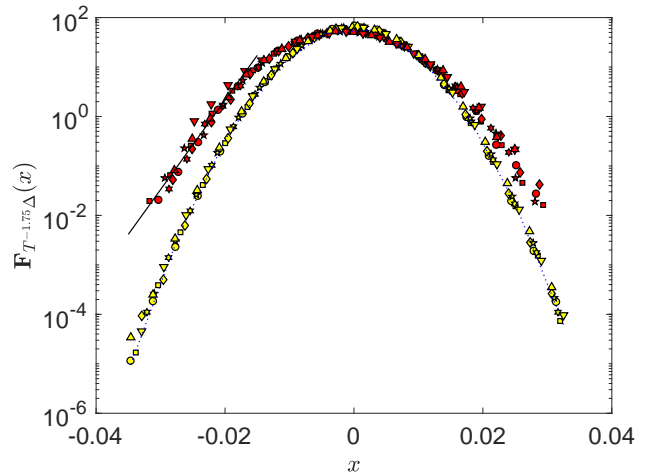

Figure 4. Seven PDFs of energy fluctuations Δ collected at aging temperatures $T = .3, .4, \ldots .7, .75$ and $.8$ are collapsed into a single Gaussian PDF by the scaling $\Delta \to T^{-\alpha}\Delta$, $\alpha = 1.75$, and plotted using a logarithmic vertical scale. The data plotted with yellow symbols are fitted by the Gaussian shown as a dotted line. This Gaussian has average $\mu_G = 0$ and standard deviation $\sigma_G \approx 6.2 \ 10^{-3}$. Data plotted with red symbols represent quake induced energy fluctuations Δ_q and, for negative values of the abscissa, have estimated probabilities close to the exponential PDF shown by the line.

PDFs feature the exponential decay given by the fitted line, which is reminiscent of the intermittent tail seen in [43]. In this case, the scaling with $T^{-\alpha}$ narrows but does not fully eliminate the spread of the data. Isothermal aging was considered in [20] for various spin-glass models and the height of the energy barriers separating the neighboring 'valleys' illustrated in Fig. 3 was studied at different temperatures. Those data were collapsed by $T^{1.8}$ scaling, a result which seems in reasonable agreement with our present findings and is likely to have the same origin.

Consider now the times of occurrence t' and t of two successive quakes, $t > t'$, and form the logarithmic time difference $\Delta \ln = \ln(t) - \ln(t') = \ln(t/t') > 0$, called for short, *log waiting time*. If quaking is a Poisson process in logarithmic time, the corresponding PDF, $F_{\Delta \ln}(x)$ is given theoretically by

$$F_{\Delta \ln}(x) = r_q e^{-r_q x}, \tag{3}$$

where r_q is the constant logarithmic quaking rate. The applicability of equation (3) has already been tested in a number of different systems, including spin-glasses [44].

The upper panel of Fig. 5 shows the empirical PDFs of our logarithmic waiting times, sampled at different temperatures and collapsed through the scaling $\Delta \ln \to T^{-\alpha}\Delta \ln$. The resulting PDF is fitted by the expression $F_{T^{-\alpha}\Delta \ln}(x) = .81 e^{-1.57x}$, which covers two decades of decay. Its mismatch with the correctly normalized expres-
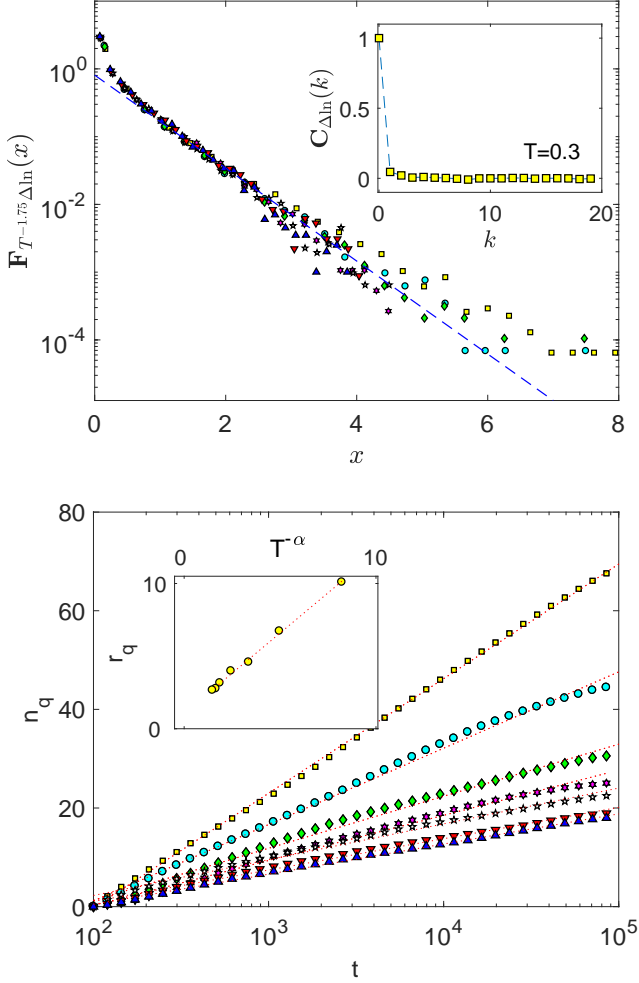
Figure 5. Upper panel. Symbols: PDF of scaled 'logarithmic waiting times' $T^{-\alpha}\Delta\ln$, $\alpha = 1.75$, for the seven aging temperatures $T = .3, .4, \ldots .7, .75$ and $.8$. Dotted line: fit to the exponential form $y(x) = .81e^{-1.57x}$. Insert: the normalized autocorrelation function of the logarithmic waiting times is very close to a Kronecker delta function $C_{\Delta\ln}(k) \approx \delta_{k,0}$. The data shown are collected at $T = .3$, but similar behavior is observed at the other investigated temperatures. Lower panel: the number of quakes occurring up to time t is plotted with a logarithmic abscissa, for all T values, with the steepest curve corresponding to the lowest temperature. Insert: The quake rate, obtained as the logarithmic slope of the curves shown in the main figure, is plotted vs. $T^{-\alpha}$, where $\alpha = 1.75$. The dotted line is a fit with slope 1.11.

sion (3) stems from the systematic deviations from an exponential decay visible for small x values. These deviations arise in turn from quakes which occur in rapid succession, and produce values $\ln(t_k/t_{k-1}) \approx 0$. The effect, which is most pronounced at early times in the simulation, roughly doubles the assessed number of quakes, and correspondingly lowers the fitted pre-factor from ≈ 1.6 to ≈ 0.8. It furthermore produces non-zero correlation values in the series of log-waiting times at $k = 1$ and, to

lesser extent, $k = 2$.

Treating closely spaced quakes as parts of the same dynamical event leads to the corrected number of quakes $n_q(t)$ occurring up to time t which is shown in the bottom panel of the figure for seven different aging temperatures. The steepest curve corresponds to the lowest temperature. The red dotted lines are linear fits of $n_q(t)$ vs. $\ln t$, and the insert shows that the logarithmic slope of the curves is well described by the function $r_q = 1.11T^{-1.75}$. We note that the logarithmic quake rate as obtained from the exponent (not the pre-factor) of the fit $y(x) = .81e^{-1.57x}$ is $r_q = 1.57T^{-1.75}$. The two procedures followed to determine the quaking rate are thus mathematically but not numerically equivalent: in the time domain they give the same $T^{-1.75}/t$ dependence of the quaking rate, but with two different pre-factors. The procedure using the PDF of the logarithmic waiting times seems preferable, due to better statistics.

Glossing over procedural difference, we write $r_q = cT^{-1.75}$ where c is a constant, and note that in our RD description the number of quakes occurring in the interval $[0, t)$ is then a Poisson process with average $\mu_N(t) = cT^{-\alpha}\ln(t)$. Qualitatively, we see that lowering the temperature decreases the log-waiting times and correspondingly increases the quaking rate. The quakes involve, however, much smaller energy differences at lower temperatures. Considering that $T^{-\alpha} \gg T^{-1}$, we see that the strongest dynamical constraints are not provided by energetic barriers. As detailed later, they are entropic in nature and stem from the dearth of available low energy states close to local energy minima. Finally, our numerical evidence fully confirms the idea that quaking is a Poisson process whose average is proportional to the logarithm of time. In other words, the transformation $t \to \ln t$ renders the aging dynamics (log) time homogeneous and permits a greatly simplified mathematical description.

B. Growth and decay of real space clusters

The mean cluster sizes shown in Fig. 6 are calculated as follows: Spins reversed by a quake are grouped into one or more spatially disjoint sets, each comprising adjacent spins. Each set is a cluster, and a first average cluster size $\overline{C_j}(t)$ is computed as the arithmetic mean of the sizes of all clusters generated at time t during the jth simulation. In a second step, our data are temporally coarse-grained by placing logarithmically equidistant time points $t_1, t_2 \ldots t_n$ within the chosen observation interval, and by treating the quakes occurring in the same log-time bin as simultaneous. The averaged cluster size $\tilde{S}_{\text{cl}}(t_k)$ is then calculated as the arithmetic mean of all the $\overline{C_j}(t)$s for which $t_{k-1} < t < t_{k+1}$. This whole procedure is repeated for different values of the aging temperature T. It follows that $\tilde{S}_{\text{cl}}(t_k)$ is the average cluster size, con-
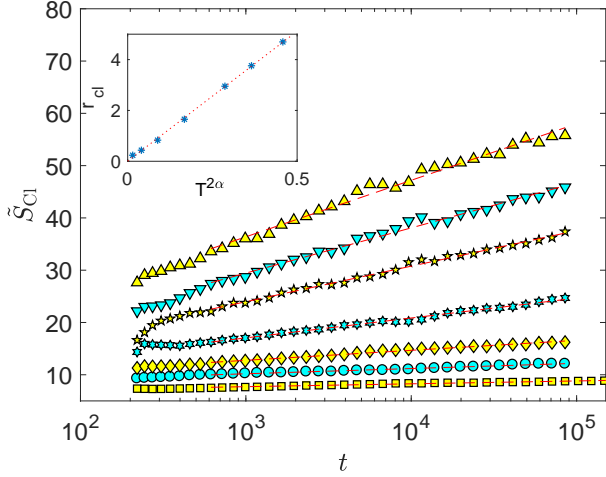
Figure 6. Main plot: the average cluster size vs. the logarithm of time. The data set, from bottom to top, are obtained at aging temperatures $T = .3, .4, .5, .6, .7, .75$ and $.8$. The red lines are linear fits of the data vs. $\ln t$. The insert shows the slope of the linear fits vs. $T^{2\alpha}$, $\alpha = 1.75$.

ditional to a quake happening near t_k. Multiplying the result with the corresponding probability r_q yields the (unconditional) average cluster size $S_{cl}(t_k)$.

Figure 6 shows that

$$
\begin{aligned}
\tilde{S}_{Cl}(t) &= r_{cl}(T) \ln t = c' T^{2\alpha} \ln t \Rightarrow \\
S_{Cl}(t) &= cc' T^{\alpha} \ln t,
\end{aligned}
\tag{4}
$$

where c and c' are positive constants. The rate at which clusters are overturned in real time, as opposed to logarithmic time, is $R_q(t) = r_q/t = cT^{-\alpha}/t$. Inserting $t = \exp(\frac{S_{Cl}T^{-\alpha}}{cc'})$ from Eq. (4), we then obtain

$$
R_q(t) = cT^{-\alpha} \exp(-\frac{S_{Cl}(t)T^{-\alpha}}{c'c}),
\tag{5}
$$

which provides the anticipated exponential relationship between the typical cluster size and the rate at which clusters of that size are overturned. Eq. (5) does not prove that a specific cluster will be overturned at a rate exponentially decreasing with its size, but is compatible with that statement, if the spatial distribution of cluster sizes is narrow.

C.   Origin of T scaling

To rationalize the T scaling of our data, we note that the conditional waiting time $W|x$ for a spin to carry out a move with energy change x is exponentially distributed with average $e^{-\frac{x}{2T}}$, see Eq. (2), i.e.

$$
p_{W|x}(t) = e^{\frac{-x}{2T}} \exp(-t\, e^{\frac{-x}{2T}}).
\tag{6}
$$

The scaled energy changes $T^{-\alpha}\Delta$ shown in Fig. 4 have a Gaussian distribution indicating that Δ is a sum of several independent terms, all sampled over short time spans of order one. Consequently, the positive energy changes selected must be of order $x \approx T$, and the negative ones are simply their reversals. Let $g(x)$ be the probability density that an energy difference x is associated to moves out of a given configuration. If the configuration is a local energy minimum, very few 'freewheeling' spins are present and, for numerically small values of x, $g(x)$ is zero for $x \leq 0$ and increases with x for $x > 0$. For configurations neighboring a local energy minimum, negative x are available corresponding to moves back to the minimum and the form of g is reversed. Glossing over the difference between local energy minima and their neighbors, we now assume that $g(x) \approx |x|^{\beta}$ for $\beta > 0$ and, for $x \propto T$, find $\Delta \propto T^{1+\beta}$, which implies that the T dependence of the sampled energy differences can be scaled away by scaling them with $T^{-\alpha}$, with $\alpha = \beta + 1$.

Energy changes from one quake to the next are plotted in the same figure, and have been similarly scaled. The $T^{-\alpha}$ scaling does not fully collapse their PDFs as expected, since the time difference between successive quakes is stochastic and typically much larger than one. The result indicates however that a trajectory triggering a quake mainly consists of a sequence of flips associated to small and reversible energy changes with the 'correct' T scaling, rather than fewer but larger energy changes associated to long waiting times. In other words, entropic barriers play a large role in the dynamics.

Since, as we just argued, the overwhelming majority of the moves are associated with small time changes, the time between two quakes is a sum of a varying, but large number of short waiting times and inherits their T^{α} dependence. The number of quakes preceding an arbitrary fixed time t is then proportional to $T^{-\alpha}$ as directly confirmed by the insert of the lower panel of Fig. (5), and indirectly by its upper panel, since the contents of the figures are mathematically equivalent.

V.   SPIN CLUSTERS AS DYNAMICAL VARIABLES

The real space clusters discussed in the previous section are mesoscopic objects which grow logarithmically in time. In this mainly theoretical section, we use them as coarse-grained variables, and show that their dynamics explains the fit of TRM data provided in [17] as well as other features of these macroscopic data. A table is included summarizing the notation used in this section.

Mathematical symbols in this section	
λ_i	i'th eigenvalue in corr. decay
w_i	weight of the corresponding term
$r_q(s)$	logarithmic rate of quakes hitting cl. of size s
b	logarithmic rate of quakes per spin
$\kappa_s(t)$	no. of quakes hitting cl. of size s in $[0,t)$
$p(s)$	prob. that a cl. of size s flips when hit
$n_{cl}(s,t)$	no. of clusters of size s present at time t
$\mu_s(t_w,t)$	average no. of hits to cl. of size s in $[t_w,t)$
μ_s	same as above

Adapting Eq.(5) of ref. [17], TRM data are described by the followin equation:

$$M_{\mathrm{TRM}}(t,t_w) = A_0\left(\frac{t}{t_w}\right)^{\lambda_0(T)} + A_1\left(\frac{t}{t_w}\right)^{\lambda_1(T)} + A_2\left(\frac{t}{t_w}\right)^{\lambda_2(T)},$$
(7)

where the pre-factors A_i and the exponents λ_i are positive respectively negative quantities. Using that λ_0 is numerically very small, one further expands the first power-law, obtaining

$$M_{\mathrm{TRM}}(t,t_w) = A_0 + a\ln(\frac{t}{t_w}) + A_1\left(\frac{t}{t_w}\right)^{\lambda_1(T)} + A_2\left(\frac{t}{t_w}\right)^{\lambda_2(T)},$$
(8)

where $a = \lambda_0 A_0 \approx -1$ is independent of temperature in the available data range. Furthermore $\lambda_1(T)$ and $\lambda_2(T)$ are weakly decreasing functions of T, with ranges close to -1 and -6, respectively. Clearly, the logarithmic approximation to the first power-law eventually fails as $t/t_w \to \infty$. However, for the data range analyzed in [17] the logarithmic term is dominant and the two remaining power-law terms only provide fast decaying transients.

Since the gauge transformation $\sigma_i \to \sigma_i(t_w)\sigma_i$, $J_{ij} \to \sigma_i(t_w)\sigma_j(t_w)J_{ij}$ maps the Thermoremanent Magnetization (TRM) into the correlation function $C(t_w,t) = \sum_i \langle\sigma(t_w)\sigma(t)\rangle$, modulo multiplicative constants, the two functions hold for our purposes equivalent information, and will be used interchangeably in the discussion.

Equation (8) was justified in [17] by the RD assumption that aging is log-time homogeneous and by then applying a standard eigenfunction expansion [47] for the magnetization autocorrelation function, alias TRM, namely

$$C(t,t_w) \propto \sum_i w(i)\exp(\lambda_i \ln(t/t_w)) = \sum_i w(i)\left(\frac{t}{t_w}\right)^{\lambda_i},$$
(9)

where $w_i \geq 0$ and $\lambda_i \leq 0$. In view of the limited accessible range of $\ln(t/t_w))$, most modes in Eq. (9) will either be frozen or have decayed to zero, leaving only a few active terms with an observable time dependence, precisely as assumed in (8).

The approach leading to Eq. (9) implicitly describes the effects of the quakes by an unspecified master equa-tion, with time replaced by its logarithm. As a consequence, the exponential decays seen in many relaxation processes are replaced by power-laws, with no connection to a critical behavior. Continuing along this line, we now construct the relevant master equation and relate its eigenvalues λ_i to real space properties uncovered in our numerical investigation. Specifically, we shall use that *i)* quakes are statistically independent events inducing cluster flips, and that *ii)* they constitute a Poisson process. Since spatial extensiveness then follows, the rate of quakes hitting a sub-system, e.g. a cluster, is proportional to the volume of the latter.

Some of the following arguments rest on unproven hypotheses, i.e. given that a quake hits a cluster of size s, the latter is assumed to flip with probability $p(s)$, a decreasing function of s, parametrised by

$$p(s) = a_0 + a_1 s^{-1} + a_2 s^{-2},$$
(10)

where all three coefficients are positive. Further below, we argue that $a_0 = a_1 = 0$.

Let $\kappa_s(t)$ denote the number of quakes hitting a cluster of size s and $n_{cl}(s,t)$ the number of such clusters present at time t. Finally, $s_{\min}$ and $s_{\max}$ denote the sizes of the smallest and the largest clusters in the system. The range of cluster sizes is constrained by the condition $\sum_{s=s_{\min}}^{s_{\max}} s\, n_{cl}(s,t) = L^3$. Finally, the total number of quakes hitting the system between t_w and t is $n_q(t) = \sum_{s=s_{\min}}^{s_{\max}} \kappa_s(t)$.

Even though the $\kappa_s(t)$ presumably share the $T^{-1.75}$ temperature dependence of $n_q(t)$, the T dependence of $p(s)$ is unknown, as is that of the cluster distribution decay, which depends on the products $\kappa_s(t)p(s)$, see Eq. (11). We therefore gloss over T dependences, but note that, in order to produce exponents with a weak T dependence [17], $p(s)$ should increase with T to counteract the strong decrease of the $\kappa_s(t)$. In other words, as the temperature decreases the number of quakes increases but their dynamical effect is reduced.

As illustrated in Fig. 1, flipping a cluster, e.g. cluster 8, eliminates all the sub-clusters present in its interior, in this case, cluster 1. To simplify our treatment, this possibility is eliminated by assuming that clusters are flipped in order of increasing size. This is reasonable if, as we shall argue, the logarithmic rate of cluster flipping decreases with cluster size. Secondly, changes in the size of a cluster induced by sub-clusters flipping in the cluster's interior are neglected. The assumptions assign a dynamical significance to the hierarchy of cluster sizes present at $t = t_w$ and allows clusters of different sizes to develop independently of each other.

Having neglected the possibility that clusters flip in the 'wrong' sequence, a cluster which flips contributes with its own size to the decay of the correlation function. Furthermore, standard arguments then imply that the number $n_{cl}(s,t)$ of clusters of size s decays exponentially

in $\kappa_s(t)$. The correlation function and, equivalently, the TRM, are given by

$$C(t_{\mathrm{w}}, t) \propto \left\langle \sum_{s=s_{\min}}^{s_{\max}} s n_{\mathrm{cl}}(s, t_{\mathrm{w}}) \exp(-p(s)\kappa_s(t)) \right\rangle, \quad (11)$$

where the constant ensuring the initial normalization has been omitted and the average $\langle \ldots \rangle$ is performed over the distribution of each $\kappa_s(t)$.

The $\kappa_s(t)$ are independent Poisson variables with expectation values

$$\mu_s(t_{\mathrm{w}}, t) = r_{\mathrm{q}}(s) \ln(t/t_{\mathrm{w}}), \quad (12)$$

where $r_{\mathrm{q}}(s)$ is the logarithmic rate of quakes impinging on a cluster of size s. The extensivity of the quaking rates implies $r_{\mathrm{q}}(s) = bs$ where b, a positive constant, is the logarithmic quake rate per spin. As a consistency check, note that

$$\sum_s r_{\mathrm{q}}(s) n_{\mathrm{cl}}(s, t) = b \sum_s s n_{\mathrm{cl}}(s, t) = bL^3 = r_{\mathrm{q}}, \quad (13)$$

the logarithmic quake rate for the whole system.

Each term of Eq. (11) can be averaged independently using

$$\langle \exp(-p(s)\kappa_s(t)) \rangle = e^{-\mu_s(t_{\mathrm{w}}, t)} \sum_{j=0}^{\infty} \frac{\mu_s(t_{\mathrm{w}}, t)^j}{j!} e^{-p(s)j},$$

$$(14)$$

which evaluates to

$$\langle \exp(-p(s)\kappa_s(t)) \rangle = \exp(-\mu_s(1 - e^{-p(s)})). \quad (15)$$

Expanding $e^{-p(s)}$ to first order, we finally obtain the contribution

$$\langle \exp(-p(s)\kappa_s(t)) \rangle \approx \exp(-\mu_s p(s)) = \left(\frac{t}{t_{\mathrm{w}}}\right)^{-bsp(s)} \quad (16)$$

to the average correlation function.

Summarizing,

$$C(t_{\mathrm{w}}, t) \propto \sum_{s=s_{\min}}^{s_{\max}} s n_{\mathrm{cl}}(s, t_{\mathrm{w}}) \left(\frac{t}{t_{\mathrm{w}}}\right)^{-bsp(s)}, \quad (17)$$

which has the same structure as Eq. (9), with the weight w_i replaced by the volume fraction $s n_{\mathrm{cl}}(s, t_{\mathrm{w}})$ occupied by clusters of size s at time t_{w} and the eigenvalue λ_i replaced by $\lambda_s = -bsp(s) = r_{\mathrm{q}}(s)p(s)$, the flipping rate of clusters of size s.

Noting that Eq. (10) entails $\lambda_s = -b(a_0 s - a_1 - a_2 s^{-1})$, we set $a_0 = 0$ on physical grounds, since the largest clusters would otherwise contribute to the fastest decay of the correlation function. The first non-zero term produces then a power-law decay term, $(t/t_{\mathrm{w}})^{-a_1 b}$, while the next term gives a whole family of power laws with different decay exponents, corresponding to the cluster size values initially represented in the system.

To regain the form given in Eq. (7) we set $a_1 = 0$ and obtain a sum of power-laws with exponents of decreasing magnitude

$$C(t_{\mathrm{w}}, t) \propto \sum_{s=s_{\min}}^{s_{\max}} s n_{\mathrm{cl}}(s, t_{\mathrm{w}}) \left(\frac{t}{t_{\mathrm{w}}}\right)^{-a_2 b/s}. \quad (18)$$

Exponents corresponding to sufficiently large clusters will, to first order in $-a_2 s^{-1} \ln(t/t_{\mathrm{w}})$, all contribute to the constant and logarithmic terms $A_0 + a \ln(t/t_{\mathrm{w}})$ seen in Eq. (8). In summary, the general form of the time dependence of the TRM data given in Eq. (8) is accounted for by our qualitative arguments, provided that a quake flips clusters of size s with probability $p(s) = a_2 s^{-2}$.

The (mainly) logarithmic decrease of the TRM data is explained using our EA model analysis in terms of large clusters associated with power-law terms with very small exponents, which can be suitably expanded. A different interpretation [4] of the same data uses the presence of crystallites of different sizes each size associated to an energy barrier and attributes the logarithmic decay of the TRM to a wide distribution of these barriers. Even though the E-A spin-glass lacks any crystallites, the presence of clusters of different sizes means that expanding the power-laws with small exponents in Eq. (18) yields, once the fast terms corresponding to small clusters have decayed,

$$M(t_{\mathrm{w}}, t) \propto A_0 - a \ln\left(\frac{t}{t_{\mathrm{w}}}\right), \quad (19)$$

where $a \propto (a_2 b)$. This expression concurs with the analysis of Ref. [17], based on the measurements of Ref. [48] if $a_2 b$ is independent or nearly independent of T. Recalling that b is the number of quakes per unit volume and per unit (log) time, an educated guess is $b \propto T^{-1.75}$, in which case the probability that a cluster of size s flips when hit by a quake should be $p(s) = a_2/s \propto T^{1.75}/s$. Note however that the T dependence of the pre-factor of the logarithmic decay is linear in Ref.[4].

Most commonly denoted by t in the literature, the 'observation time' elapsed after t_{w} is, in our notation, denoted by $t_{\mathrm{obs}} \stackrel{\text{def}}{=} t - t_{\mathrm{w}}$. Interesting geometrical features of the spin glass phase, such as the size of correlated domains [28, 29], are associated to the 'relaxation rate' $S_{\mathrm{R}}(t_{\mathrm{obs}}, t_{\mathrm{w}})$, defined as the derivative of the TRM with respect to $\ln t_{\mathrm{obs}}$ [3], and in particular to its broad maximum at $t_{\mathrm{obs}} \approx t_{\mathrm{w}}$. To see the origin of the latter, we derive the relaxation rate from Eq. (9) as

$$S_{\mathrm{R}}(t_{\mathrm{obs}}/t_{\mathrm{w}}) \propto \frac{t_{\mathrm{obs}}}{t_{\mathrm{w}}} \sum_s |\lambda_s| w_s \left(\frac{t_{\mathrm{obs}} + t_{\mathrm{w}}}{t_{\mathrm{w}}}\right)^{\lambda_s - 1}, \quad (20)$$

which is the product of an increasing pre-factor $\frac{t_{\mathrm{obs}}}{t_{\mathrm{w}}}$ and a sum of decreasing terms $\left(\frac{t_{\mathrm{obs}} + t_{\mathrm{w}}}{t_{\mathrm{w}}}\right)^{\lambda_s - 1}$. Each of these

terms has a maximum at $t_{\mathrm{obs}}/t_{\mathrm{w}} = -1/\lambda_s$, and, together, they give rise to the broad maximum near $t = t_{\mathrm{w}}$ experimentally observed for the relaxation rate [3].

Using $\lambda_s = -a_2 b/s$, and recalling that $w_s = s n_{\mathrm{cl}}(s, t_{\mathrm{w}})$, we find that the relaxation rate for the value $t_{\mathrm{obs}} = 2t_{\mathrm{w}}$ commonly used in the literature is

$$S_{\mathrm{R}}(2) \propto \sum_{s=s_{\min}}^{s_{\max}} n_{\mathrm{cl}}(s, t_{\mathrm{w}}) 3^{-a_2 b/s} \propto \langle 3^{-a_2 b/s} \rangle, \qquad (21)$$

where the brackets denote an average over the size distribution of clusters present at $t = t_{\mathrm{w}}$. Importantly, Eq. (20) and (21) show that the relaxation rate and its maximum both gauge the characteristic size of the clusters, or domains, present in the system at time t_{w}.

VI. IMPLICATIONS OF $T^{1.75}$ SCALING

The $T^{1.75}$ dependence of energy changes characterizing isothermal trajectories at different temperatures (see Fig. 4) implies that the barriers separating the parts of configuration space where these trajectories unfold are not easily surmounted by the thermal $\mathcal{O}(T)$ fluctuations available in quasi-equilibrium states.

To the best of the authors' knowledge, this anomalous scaling has not been noticed in other numerical simulations, except for a brief mention in Ref.[20], where a slightly different scaling exponent was found. However, as we argue below, the behavior fits and partly explains the rejuvenation and memory effects experimentally seen in spin-glasses [45, 46] under a change of temperature protocol.

In [45], the imaginary part of the magnetic susceptibility is measured at high frequency, $\omega > 1/t_{\mathrm{w}}$, while the system is cooled at constant rate through a range of low temperatures. As such, this protocol produces an out of phase (pseudo-)equilibrium magnetic susceptibility $\chi''(\omega, T)$, which is utilized as a reference or master curve. Importantly, the cooling process is halted at temperature T_1 and the system is allowed to age isothermally for several hours, leading to a decrease, or 'dip', of the susceptibility away from the master curve. When cooling is resumed, the measurements soon return to that curve, a rejuvenation effect implying that states seen during the aging process at T_1 have little influence on those seen at other temperatures. Furthermore, a second aging stop at a lower temperature T_2 produces a second dip. The striking memory behavior of the system is revealed when the system, continuously re-heated without any aging stops, re-traces the dips of the susceptibility previously created at T_1 and T_2. Similar rejuvenation and memory behavior is observed in TRM traces [46]. These experiments show that aging trajectories at different, not too close, temperatures are dynamically disconnected. Our numerical data point, as anticipated, in the same direction and

offer at the same time an explanation of the rejuvenation part of the experimental findings.

VII. SUMMARY & DISCUSSION

This work's main focus is to buttress Record Dynamics (RD) [16–19, 34] as a general method to coarse-grain aging processes, by analyzing numerical simulations from a model with quenched randomness. Spin glasses are iconic systems, where a wealth of fascinating phenomena illustrating central aspects of complexity have been experimentally uncovered (see [2, 3] and references therein), and the E-A model was an obvious choice.

For historical reasons, traditional interpretations of both numerical and experimental spin-glass data rely on adaptations of equilibrium concepts, e.g. critical behavior and other properties of either [2] the Parisi solution [49] of the mean field Sherrington-Kirkpatrick model [50], or [3] the real space description of the E-A model [22] proposed by Fisher and Huse [1]. Since RD relies on the statistical properties of non-equilibrium events, the picture emerging from our investigations unsurprisingly differs in some respects from more established descriptions.

RD tacitly assumes the existence of a hierarchy of free energy barriers in configuration space [19, 34] which, however, bears no direct relation to mean-field spin-glass models and rests on general arguments of dynamical nature [13, 53], exemplified by a coarse-grained discrete toy-model of 'valleys within valleys', i.e. thermal hopping on a tree structure [14].

A connection between the ultrametrically organized pure states [49] of the SK model, which are intrinsically stable equilibrium objects, and the metastable states of real spin glasses requires a degree of funambulism. The needed tight-rope [51] is provided in Ref. [52], where the spin-glass configuration space is depicted as a hierarchically organized set of metastable states.

Treating an aging spin glass as a critical ferromagnet in disguise is, we argued, a dubious undertaking on two counts: *i)* Even though the energy difference between two metastable states is associated to a domain wall, the dynamical barriers that hinder a reversal of the domain orientation are not. They are instead associated to the interior of the domain. *ii)* While the dynamics of a 3D spin glass looks critical when T_c is approached from above, once below T_c thermal equilibration is chimeric and the physical relevance of the critical temperature is moot.

Some descriptions, see e.g. [55], model aging dynamics as a random walk in a configuration space fraught with traps whose exit times feature a long tailed distribution [54] of unspecified origin. For a detailed discussion of continuous time random walks and 'weak ergodicity breaking' vs RD, we refer to [18]. Here we just note that RD traps all have a finite depth, i.e. a finite average

exit time, but are typically visited in order of increasing depth. Last but not least, the quake, i.e. jump, statistics in RD is predicted from configuration space properties, rather than simply assumed.

Keeping our focus in mind, the experimental results discussed in some detail [4, 17, 45, 46] are all directly connected to our findings. Secondly, variants of the E-A model, e.g. binary coupling distributions, are not discussed. Considering RD's broad applicability, it seems plausible that such models would yield qualitatively similar results. Some technical adjustments would however be needed for our definition of clusters, as the ground state is degenerated beyond a global inversion symmetry.

In a spin glass context, RD has been used to describe TRM experiments [17] and numerical heat exchange data [43]. In the present investigation, quakes are operationally defined by associating them to record values of a suitably defined 'energy barrier' function sampled during the simulations, as graphically illustrated by Fig. 3. That these quakes are a Poisson process whose average grows with the logarithm of time is explicitly verified in Fig. 5, which confirms the basic assumption on which RD relies.

Neglecting easily reversed single spin excitations produces the coarse-grained picture we use, where every low temperature configuration appears as a collection of adjacent spin clusters, each oriented as one of the two ground states of the E-A model. Clusters are identified from simulational data as groups of spins which change direction during a quake while keeping their relative orientations unchanged. On average, the size of spin clusters overturned at time t grows as $\ln t$ and the rate at which a cluster is overturned decreases exponentially with its size. This relation subsumes the effect of both entropy and energy barriers and establishes a connection with our model of dense colloids [32, 33].

A so far unnoticed property of the E-A model seen in Figs. 4 and 5 is that aging data, e.g. energy differences and logarithmic waiting times, collected at different (low) temperatures can be collapsed by scaling them with $T^{-1.75}$. This property is explained with the form $g(x) \propto |x|^{3/4}$ which, for $x \approx 0$ is assumed to describe the energy changes associated to moves to and from a local energy minimum configuration. In the simulations, the WTM's dwells near local energy minima, where it repeatedly samples this type of energy fluctuations. We argue that the dearth of available moves with a low associated energy change can explain the rejuvenation part of memory and rejuvenation experiments [45, 46]: Simply put, states explored during isothermal aging at different temperature are separated by large dynamical barriers of entropic nature, and these barriers are not easily overcome by thermal equilibrium fluctuations, which scale linearly with T.

Finally, an approximate real-space analytical description is developed using growing clusters as mesoscopic dynamical variables. Important elements are that the logarithmic rate of quakes is an extensive and time independent quantity and that, given that a cluster is hit by a quake, it flips with a probability inversely proportional to its size. Unlike the first assumption, the second is only supported *a posteriori* by the formula it produces, which empirically describes TRM decay data [17].

Importantly, the power-law terms vanish fairly rapidly and the remaining logarithmic decay, which formally arises by expanding a possibly large group of power-laws with small exponents, has a pre-factor which is T independent, as in the experimental data analysis of [17] but in contrast with the formula given in [4]. A similar behavior [6, 56] is seen in the temperature independence of the magnetic creep rate of high T_{c} superconductors.

By focussing on non-equilibrium quakes and their statistics, several real space implications are brought forth of the hierarchical energy landscape organization which RD relies on, and a clear relation emerges between configuration and real space pictures of spin-glass dynamics, namely that increasingly scales in Hamming and Euclidean distance become relevant as increasing dynamical barriers are overcome.

---

[1] Daniel S. Fisher and David A. Huse. Nonequilibrium dynamics of spin glasses. *Phys. Rev. B*, 38:373–385, 1988.

[2] Eric Vincent. Ageing, rejuvenation and memory: The example of spin glasses. *Lect. Notes Phys.*, 716:7–60, 2007.

[3] Per Nordblad and Peter Svedlindh. Experiments on spin glasses, in Spin Glasses and Random Fields. Edited by A. P. Young, page 1. *World Scientific*, 1997.

[4] Samaresh Guchhait, Gregory G. Kenning, Raymond L. Orbach and Gilberto F. Rodriguez. Spin glass dynamics at the mesoscale. *Phys. Rev. B*, 91:014434, 2015.

[5] Gary L. Hunter and Eric R. Weeks. Free-energy landscape for cage breaking of three hard disks. *Physical Review E*, 85(3, 1), MAR 23 2012.

[6] Mario Nicodemi and Henrik Jeldtoft Jensen. Creep of superconducting vortices in the limit of vanishing temperature: A fingerprint of off-equilibrium dynamics. *Phys. Rev. Lett.*, 86:4378–4381, 2001.

[7] P. Jönsson, M.F. Hansen, and P. Nordblad. Nonequilibrium dynamics in an interacting fe-c nanoparticle system. *Phys. Rev. B*, 61:1261–1266, 2000.

[8] Nikolaj Becker and Paolo Sibani. Evolution and non-equilibrium physics: A study of the Tangled Nature Model. *EPL*, 105:18005, 2014.

[9] Christian Walther Andersen and Paolo Sibani. Tangled nature model of evolutionary dynamics reconsidered: Structural and dynamical effects of trait inheritance. *Phys. Rev. E*, 93:052410, 2016.

[10] Ariel Amir, Yuval Oreg, and Yoseph Imry. On relaxations and aging of various glasses. *Proceedings of the National Academy of Sciences*, 109(6):1850–1855, 2012.

[11] Paolo Sibani and Gregory G. Kenning. Origin of end-of-

aging and subaging scaling behavior in glassy dynamics. *Phys. Rev. E*, 81:011108, Jan 2010.

[12] R. G. Palmer, D. L. Stein, E. Abraham, and P. W. Anderson. Models of hierarchically constrained dynamics for glassy relaxation. *Phys. Rev. Lett.*, 53:958–961, 1984.

[13] Karl Heinz Hoffmann and Paolo Sibani. Diffusion in hierarchies. *Phys. Rev. A*, 38:4261–4270, 1988.

[14] Paolo Sibani and Karl Heinz Hoffmann. Hierarchical models for aging and relaxation of spin glasses. *Phys. Rev. Lett.*, 63:2853, 1989.

[15] P. Sibani, J.C. Schön, P. Salamon and J.-O. Andersson. Emergent hierarchical structures in complex system dynamics. *Europhys. Lett.*, 22:479–485, 1993.

[16] Paul Anderson, Henrik Jeldtoft Jensen, L.P. Oliveira and Paolo Sibani. Evolution in complex systems. *Complexity*, 10:49–56, 2004.

[17] Paolo Sibani, G. F. Rodriguez and G. G. Kenning. Intermittent quakes and record dynamics in the thermoremanent magnetization of a spin-glass. *Phys. Rev. B*, 74:224407, 2006.

[18] Paolo Sibani. Coarse-graining complex dynamics: Continuous time random walks vs. record dynamics. *EPL*, 101:30004, 2013.

[19] Paolo Sibani and Henrik Jeldtoft Jensen. *Stochastic Dynamics of Complex Systems: from Glasses to Evolution.* Imperial College Press, 2013.

[20] J. Dall and P. Sibani. Exploring valleys of aging systems: the spin glass case. *The European Physical Journal B - Condensed Matter and Complex Systems*, 36(2):233–243, 2003.

[21] S. Boettcher and P. Sibani. Comparing extremal and thermal explorations of energy landscapes. *The European Physical Journal B - Condensed Matter and Complex Systems*, 44:317–326, 2005.

[22] S. F. Edwards and P. W. Anderson. Theory of spin glasses. *J. Phys. F*, 5:965-974, 1975.

[23] Ludovic Berthier and Jean-Philippe Bouchaud. Geometrical aspects of aging and rejuvenation in the Ising spin glass: A numerical study. *Phys. Rev. B*, 66:054404, 2002.

[24] Paolo Sibani and Peter Schriver. Local phase-space structure and low-temperature dynamics of short-range Ising spin glasses. *Phys. Rev. B*, 49:6667-6671, 1994.

[25] Stefan Schnabel and Wolfhard Janke. Distribution of metastable states of Ising spin glasses. arXiv:1802.04514.

[26] Kenneth S. Schweizer. Dynamical fluctuation effects in glassy colloidal suspensions. *Current Opinion in Colloid Interface Science*,12:297-306, 2007.

[27] F. Belletti et al. Janus Collaboration. *J. Stat. Phys.*, 135:1121, (2009)

[28] M. Baity-Jesi et al. Janus collaboration. *Phys. Rev. Lett.*, 118:157202, 2017.

[29] Y. G. Joh, R. Orbach and G. G. Wood Extraction of the Spin Glass Correlation Length. *Phys. Rev. Lett.*, 82:438–441, 1999.

[30] Samaresh Guchhait and Raymond L. Orbach. Magnetic Field Dependence of Spin Glass Free Energy Barriers. *Phys. Rev. Lett.* 118:157203, 2017.

[31] Qiang Zhai, David C. Harrison, Daniel Tennant, E. Dan Dalhberg, Gregory G. Kenning and Raymond L. Orbach. Glassy dynamics in CuMn thin-film multilayers. *Phys. Rev. B*, 95:054304, 2017.

[32] Stefan Boettcher and Paolo Sibani. Ageing in dense colloids as diffusion in the logarithm of time. *J. Phys.: Cond. Matter*, 23:065103, 2011.

[33] Nikolaj Becker, Paolo Sibani, Stefan Boettcher, and Skanda Vivek. Temporal and spatial heterogeneity in aging colloids: a mesoscopic model. *J. Phys.: Cond.. Matter*, 26:505102, 2014.

[34] Dominic M. Robe, Stefan Boettcher, Paolo Sibani and Peter Yunker. Record dynamics: Direct experimental evidence from jammed colloids. *EPL*, 116:38003, 2016.

[35] Dominic M. Robe and Stefan Boettcher. Two-Time Correlations for Probing the Aging Dynamics of Jammed Colloids. *ArXiv*:1802.05350, 2018.

[36] C. M. Newman and D. L. Stein. Non-Mean-Field Behavior of Realistic Spin Glasses. *Phys. Rev. Lett.*, 76:515-518, 1986.

[37] Pierluigi Contucci and Cristian Giardinà. Perspectives on Spin Glasses. *Cambridge University Press*, 2012.

[38] Helmuth G. Katzgraber, Mathias Körner and P. Young. Universality in three-dimensional Ising spin glasses: A Monte Carlo study. *Phys. Rev. B*, 73:224432, 2006.

[39] J. Dall and P. Sibani. Faster Monte Carlo simulations at low temperatures. the waiting time method. *Computer Physics Communications*, 141:260–267, 2001.

[40] Helmuth G. Katzgraber, Simon Trebst, David A. Huse and Matthias Troyer. Feedback-optimized parallel tempering Monte Carlo *Journal of Statistical Mechanics: Theory and Experiment* , 2006:P03018, 2006.

[41] S. Boettcher and A. G. Percus. Optimization with Extremal Dynamics. *Phys. Rev. Lett.*, 86:5211, 2001.

[42] Bernd A. Berg, Alain Billoire and Wolfhard Janke. Spin Glass Overlap Barriers in Three and Four Dimensions. *Phys. Rev. B*, 61:12143, 2000.

[43] P. Sibani and H. Jeldtoft Jensen. Intermittency, aging and extremal fluctuations. *EPL* , 69:563, 2005.

[44] P. Sibani. Linear response in aging glassy systems, intermittency and the Poisson statistics of record fluctuations. *The European Physical Journal B*, 58:483–491, 2007.

[45] K. Jonason, E. Vincent, J. Hammann, J. P. Bouchaud, and P. Nordblad. Memory and Chaos Effects in Spin Glasses. *Phys. Rev. Lett.*, 81:3243, 1998.

[46] R. Mathieu, M. Hudl and P. Nordblad. Memory and rejuvenation in a spin glass. *EPL* , 90:67003, 2010.

[47] N. G. Van Kampen. Stochastic processes in physics and chemistry. *North Holland, Amsterdam*, 2006.

[48] G. F. Rodriguez, G. G. Kenning, and R. Orbach. Full Aging in Spin Glasses. *Phys. Rev. Lett.* 91:037203, 2003.

[49] G. Parisi. Order parameter for spin glasses. *Phys. Rev. Lett.* 50:1946, 1983.

[50] David Sherrington and Scott Kirkpatrick. Solvable Model of a Spin-Glass. *Phys. Rev. Lett.* 35:1792, 1975.

[51] S. L. Ginzburg. Nonergodicity and nonequilibrium character of spin glasses. *Sov. Phys. JETP*, 63:439, 1986.

[52] M. Lederman, R. Orbach, J.M. Hamman, M. Ocio and E. Vincent. Dynamics in spin glasses. *Phys. Rev. B*, 44:7403, 1991.

[53] H. A. Simon. The architecture of complexity.. *Proc. of the American Philosophical Society*, 106:467, 1962.

[54] J.P. Bouchaud. Weak ergodicity breaking and aging in disordered systems. *J. Phys. I France*, 2:1705, 1992.

[55] E. Vincent, J. P. Bouchaud, D. S. Dean, and J. Hammann. Aging in spin glasses as a random walk: Effect of a magnetic field. *Phys. Rev. B*, 52:1050, 1995.

[56] L. P. Oliveira, Henrik Jeldtoft Jensen, Mario Nicodemi, and Paolo Sibani. Record dynamics and the observed temperature plateau in the magnetic creep-rate of type-II superconductors *Phys. Rev. B* 71:104526, 2005.